ACS Photonics

Article

pubs.acs.org/journal/apchd5

Far-Field Subdiffraction Imaging of Semiconductors Using Nonlinear Transient Absorption Differential Microscopy

Ning Liu,[†,‡] Mahendar Kumbham,[†,‡] Isabel Pita,[†,‡] Yina Guo,[‡] Paolo Bianchini,[§] Alberto Diaspro,[§,∥] Syed A. M. Tofail,[†,‡] André Peremans,[⊥] and Christophe Silien*[,†,‡]

[†]Department of Physics and Energy and [‡]Materials and Surface Science Institute, University of Limerick, Limerick V94 T9PX, Ireland

[§]Department of Nanophysics, Istituto Italiano di Tecnologia, Genoa 16163, Italy

[∥]Department of Physics, University of Genoa, Genoa 16126, Italy

[⊥]Centre de Recherches en Physique de la Matière et du Rayonnement, Université de Namur, Namur 5000, Belgium

Supporting Information

ABSTRACT: Label-free absorption spectroscopies are frontline techniques to reveal the spectral fingerprint, composition and environment of materials and are applicable to a wide range of samples. In an effort to improve the spatial resolution of far-field absorption microscopy, which is limited by the diffraction of light, an imaging technique based on transient absorption saturation has recently been developed. Here we report a far-field transient absorption microscopy that does not require the sample to exhibit saturable absorption to break the diffraction barrier. By alternating the wavefront of the pump beams and exploiting a nonlinearity in the transient absorption intrinsic to semiconductors, we demonstrate imaging, beyond the diffraction limit, in CdSe nanobelts. This differential technique is applied for label-free super-resolution absorption microspectroscopy.

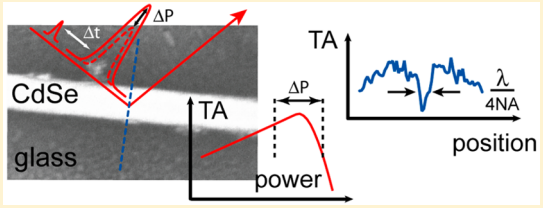

KEYWORDS: *super-resolution, label-free, microspectroscopy, bleaching, induced absorption, nanowire, pump−probe, cadmium selenide*

The application of fast and ultrafast pulsed laser sources in absorption spectroscopy allows the measurement of transient absorption (TA) phenomena with picosecond and femtosecond temporal resolution. TA microscopy has been used for the detection of single metal and semiconductor nanoparticles that are not detected by conventional means such as Rayleigh scattering.[1] The scope of this technique is now expanding beyond the spectral and temporal resolution, as it suppresses the averaging in macroscopic samples of nanomaterials and uniquely reveals environmental influence.[2] The scheme behind the subwavelength TA microscopy demonstrated on graphene nanoplatelets by Wang et al.[3] relies on a doughnut-shaped saturation beam quenching the saturable absorption and the TA-bleaching signal in the periphery of a diffraction-limited volume. The reduction in the spatial dimension of the effective TA point-spread function (PSF) depends on the doughnut saturation beam being intense and higher than the absorption saturation threshold of the material under microscopic investigation. This scheme is analogous to the reversible saturable fluorescent transitions (RESOLFT)[4−8] techniques, which are known to break the diffraction barrier of visible light with the help of fluorescent labels. Saturation in surface plasmon scattering of small Au nanoparticles has also been observed, and super-resolution imaging exploiting the phenomena was demonstrated.[9] On the other hand, the scope of TA microscopy is to measure the absorption bleaching and thus to map below the diffraction limit intrinsic spectral features exploitable in most specimens.[10]

To extend the field of applications of subwavelength resolution TA techniques beyond the requirement of optical transition saturation,[3] we introduce an alternative scheme here. First, the subdiffraction TA microscopy proposed in our scheme exploits a nonlinearity in the transient absorption, which appears as a change in the transient absorption rate with the increase of pump intensity (Figure 1a), but does not require saturable absorption. Second, this scheme further relies on differential illumination, akin to those theoretically discussed earlier by our group in the context of transient absorption and spontaneous absorption microspectroscopy[11,12] and those demonstrated by others for imaging fluorescence in labeled samples.[13,14] In addition, since both pump and probe beams are wavelength degenerated, this technique can be applied to a variety of wavelengths absorbed by the sample.

As illustrated in Figure 1a, the differential transient absorption (DTA) scheme involves measuring the difference between transient absorption signals induced by two pumps. When the pump intensity is below the nonlinear threshold p_0 (Figure 1a(I)), the DTA is possible with the alternation of Gaussian and doughnut pumps, with an improvement in spatial resolution determined by the doughnut pump node dimensions. Super-resolution is further realized from the additional spatial frequencies (with respect to those defined by optical diffraction) that are introduced in the amplitude PSF[15] when

Received: December 14, 2015
Published: February 3, 2016

DOI: 10.1021/acsphotonics.5b00716
ACS Photonics 2016, 3, 478−485

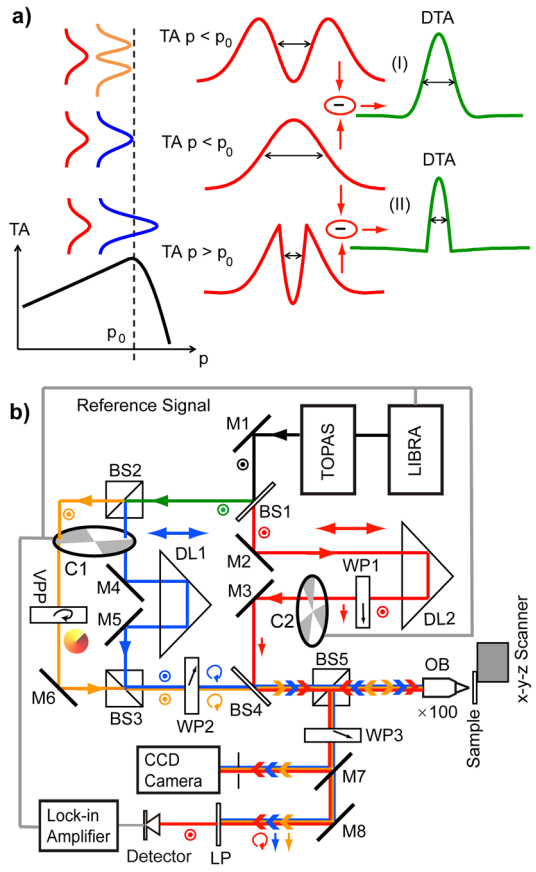

Figure 1. Differential transient absorption scheme and experimental setup. (a) Differential transient absorption (DTA) scheme exploited in our experiment at different pump (p) intensity. Below p_0, the DTA signal refers to the change in absorption of the probe by Gaussian and doughnut-shaped pumps (I). Above p_0, the DTA signal refers to the change in absorption of probe by two Gaussian pumps at intensities below and above p_0 (II). The curves in red show the probes (before and after interaction with the pumped sample), those in orange and blue show respectively the doughnut and Gaussian pumps, and those in green show the DTA signals. (b) Schematics of the DTA experimental setup. Gray lines indicate electronic reference signal paths. Blue, orange, and red lines represent respectively the Gaussian pump, doughnut pump, and Gaussian probe optical paths. M = mirror, BS = beam splitter, C = chopper wheel, DL = delay line, WP = wave plate, OB = objective, LP = linear polarizer, and VPP = vortex phase plate.

exploiting TA nonlinearity, for example by using two Gaussian pumps in alternation, one of power below the nonlinear threshold p_0 and one just above (Figure 1a(II)), and thereby confining the nonlinear response to dimensions less than the pump beam diameter (see also Supporting Information S1). The enhancement of spatial resolution is visualized in the DTA images from the differential signal being maximum at the center of the two pumps and zeroed at their periphery, where both pump absorption-induced effective amplitude PSF are of same magnitude. Breaking away from the RESOLFT-based schemes, the confinement and thus spatial resolution are maximum at the threshold power p_0 and decrease beyond.

This nonlinear TA differential microscopy scheme is demonstrated for CdSe nanobelts as an example. These nanobelts cannot be taken to an absorption saturation, as they exhibit absorption bleaching and induced absorption at different pump intensities. Spectral and temporal features in the transient absorption similar to those found in the CdSe nanobelts are found in many other semiconductors and insulators such as Si, InGaAsP, CdS, CuS, Ag_2S, and $SrTiO_3$,[16−22] which warrant that our subdiffraction DTA microscopy is applicable to a vast range of materials.

MATERIALS AND METHODS

Growth of CdSe Nanobelts. The thicker CdSe nanobelts were grown by chemical vapor deposition, using similar steps as detailed in ref 23. In general, CdSe powder is placed in an alumina boat, which is then put in the middle of a quartz tube furnace (single zone, Elite Thermal Systems). Au (5 nm)-coated Si substrate is placed at the downstream side of the tube. The furnace is first pumped down with a rotary pump for 30 min. Ar gas is then introduced in the tube with a flow rate of 50 sccm while the pump is kept on. After 20 min, the furnace is heated quickly to 690 °C and kept at this temperature for 30 min for CdSe nanobelt growth. During the growth, the Si sample is kept at a temperature of 500−600 °C. The CdSe nanobelts grown this way are 100−300 nm thick, 140−500 nm wide, and 5−15 μm long.

Thinner CdSe nanowires (2−6 μm long, 20−100 nm wide) were synthesized by altering the amount of reactants described in a well-documented CdSe nanorod synthesis procedure.[24,25] A 2 g amount of cadmium oxide, 0.71 g of tetradecylphosphonic acid (TDPA), 2 g of n-hexylphosphonic acid (HPA), and 3 g of trioctylphosphine oxide (TOPO) were added to a three-neck flask. The mixture was placed in an argon atmosphere, under rapid magnetic stirring, and heated to 120 °C. The system was then evacuated for 1 h. Following this the mixture was heated to 300 °C in an argon atmosphere to allow the CdO to decompose. Once this temperature was reached, 1.5 g of trioctylphosphine (TOP) was injected in and the temperature was further raised to 310 °C. A 500 μL amount of selenium/TOP solution (0.875 g Se/5 g TOP stock) was quickly injected into the flask, and the solution was left for 7 min to allow the CdSe nanowires to grow. The growth was then halted by removing the heating mantle, and 3 mL of toluene was injected into the solution at 80 °C to stop the reaction. The nanowires were then washed in toluene and 2-propanol three times through a centrifuge at 3000 rpm. The nanowires were then redispersed in 2-propanol for further use.

Experimental Setup. The DTA is implemented using a wavelength-degenerate optical pump−probe scheme, with all the beams generated by a single optical parametric amplifier (OPA) (Light Conversion SHBC-TOPAS-400-WL) delivering a nearly Fourier-transformed picosecond (2 ps) signal tunable between 400 and 800 nm and pumped by a femtosecond regenerative Ti-sapphire amplifier (Coherent LIBRA; 1 kHz, 800 nm). The power at the sample was kept below 0.25 μW, below the damage threshold of the CdSe nanobelts. The vertically polarized nearly-Gaussian OPA signal is first split 10:90 in two beams, with the least energetic portion used as probe beam. The most energetic portion is further split 50:50 in two pump beams. One pump beam passes through a 2π vortex phase plate (RPC Photonics) to realize a doughnut intensity profile on the sample and is coaligned using a beam splitter with the second pump beam kept Gaussian. The pump beam's polarization is changed to circular with a tunable quarter-wave plate. The probe beam polarization is changed to horizontal with a tunable half-wave plate. Ten percent of the probe beam is finally coaligned with 90% of the doughnut and Gaussian pump beams, and the three beams are focused with a

DOI: 10.1021/acsphotonics.5b00716
ACS Photonics 2016, 3, 478−485

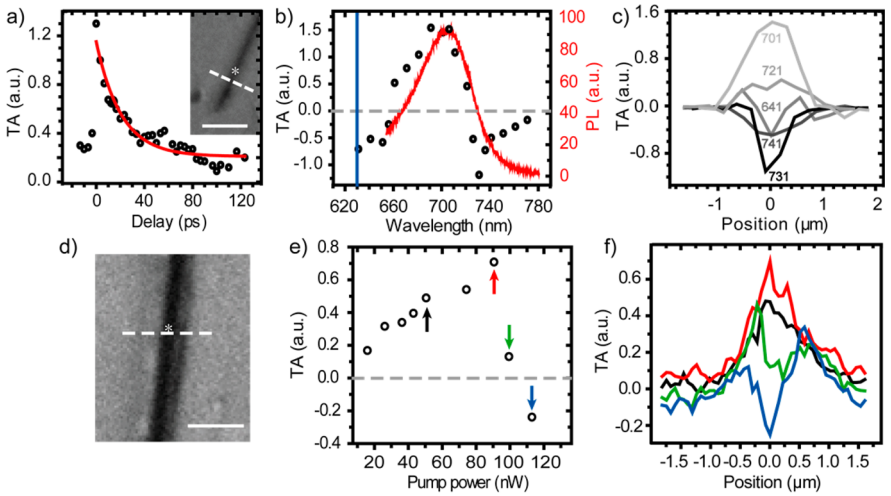

Figure 2. Single CdSe nanobelt transient absorption. (a) TA amplitude vs probe delay at 679 nm measured at the center of the CdSe nanobelt shown in the wide-field image in the inset (pump = 47 nW; probe = 14 nW). Scale bar indicates 3 μm. (b) TA amplitude vs wavelength recorded at the center of the NB1 shown in (a) (pump = 80 nW; probe = 28 nW). (c) TA microscopy cross sections recorded along the dashed line in (a) at various wavelengths indicated in the graph. (d) Wide-field image of another CdSe nanobelt. Scale bar is 2 μm. (e) TA amplitude vs Gaussian pump power recorded at 679 nm at the center of NB in (d) (probe = 9 nW). (f) TA microscopy cross sections recorded along the dashed line in (d) and matching with the black, red, green, and blue arrows in (e). All TA data were recorded with only the Gaussian pump enabled.

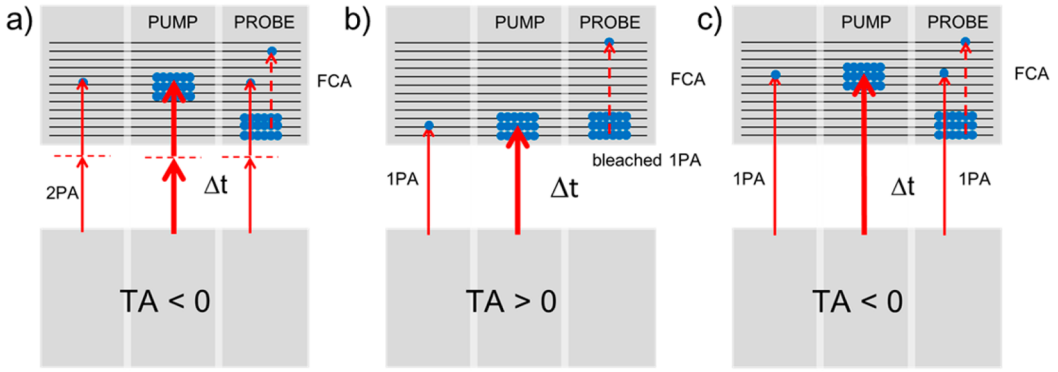

Figure 3. Energy band excitation diagrams. (a) Left: Probe absorption by two-photon absorption (2PA) at long wavelength with sample at equilibrium. Middle: Pump absorption by 2PA creating a large carrier density in the conduction band. Right: Probe absorption by 2PA and free carrier absorption (FCA) after Δt and intraband decay of the carrier at the band edge. (b) Left: Probe absorption by 1PA with sample at equilibrium. Middle: Pump absorption by single photon (1PA), creating a large carrier density at the conduction band edge. Right: Probe absorption by FCA with 1PA bleached after Δt. One PA bleaching and FCA compete with TA > 0 at low pump power and TA < 0 at high pump power. (c) Left: Probe absorption by 1PA with sample at equilibrium for short wavelength. Middle: Pump absorption by 1PA, creating a large carrier density far in the conduction band. Right: Probe absorption by 1PA and FCA after Δt and intraband decay of the carrier at the band edge.

100× objective (Olympus, NA = 0.9) onto the sample. The probe, Gaussian pump, and doughnut pump powers were individually controlled using neutral density filters, and the two pumps are made to illuminate the sample in alternation by using a single chopper wheel rotating at f_1 = 500 Hz. A second chopper wheel at f_2 = 333 Hz modulates the probe. The backscattered light is collected and directed into a fast silicon photodiode (Thorlabs DET10A/M) and processed with a lock-in amplifier referenced at $f_1 - f_2$ = 167 Hz for phase-sensitive heterodyne detection of the TA and DTA signals (see Supporting Information S2), while scanning the sample with a piezoscanner. A quarter-wave plate and a linear polarizer are placed before the photodiode to minimize the pump power intake and improve the detection sensitivity; the first changes the polarization of the probe beam to circular and that of the pump beams to linear, and the second blocks about 90% of the pump beams. A CCD camera is available to verify the three-beam coalignment on the sample and for wide-field imaging when used in conjunction with a white LED illuminating the back of the sample. The PL spectrum can be selectively directed to a spectrograph (Acton Princeton Instrument). SEM images were recorded with a Hitachi S-4800 with the beam set at 5 kV.

RESULTS AND DISCUSSION

The experimental setup and the detection technique are depicted in Figure 1b (see also Materials and Methods and Supporting Information S2). The CdSe nanobelts were drop cast on a microscope glass slide. Single nanobelts were identified by wide-field visible light imaging. In all measurements, the pump and probe beams originate from a single laser beam, separated by beam splitters. Therefore, their wavelengths are identical. Figure 2a shows the evolution of the TA signal as a function of the probe delay recorded at the center of one of the nanobelts at 679 nm using only the Gaussian pump and probe beams. The excitation relaxes in ca. 22 ± 2 ps, estimated by fitting the experimental data points to a single exponential,

DOI: 10.1021/acsphotonics.5b00716
ACS Photonics 2016, 3, 478−485

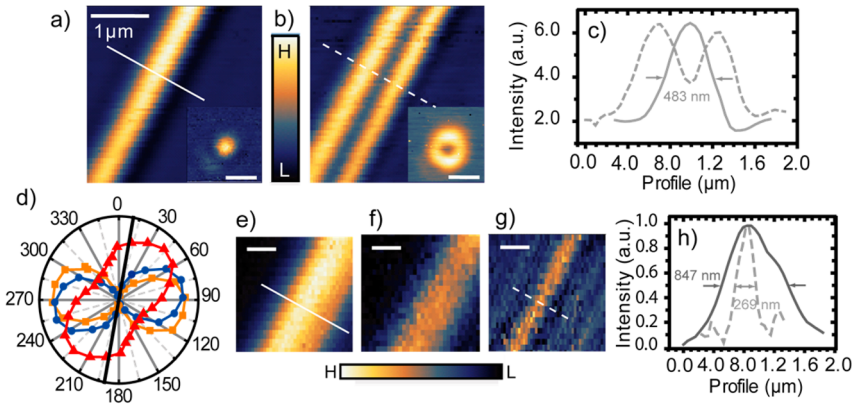

Figure 4. Transient absorption and differential transient absorption microscopy of a CdSe nanobelt. (a) Backscattered microscopy of NB1 at 679 nm using the Gaussian pump beam (13 nW) without detection polarizer. Inset: Backscattered microscopy of a gold nanoparticle using the same beam (scale bar: 500 nm). (b) Same as (a) using the doughnut pump beam (13 nW). (c) Cross section extracted from the images in panels (a) and (b). The profiles are normalized so that their maximum matches. (d) Polarization plot measured on the Gaussian (blue) and doughnut pump (orange) and probe (red) beams before LP. (e–g) Gaussian TA (pump = 53 nW; probe = 7 nW), doughnut TA (pump = 65 nW; probe = 7 nW), and DTA microscopy (Gaussian = 53 nW, doughnut = 65 nW, probe = 7 nW) of the nanobelt (scale bars 500 nm). (h) Cross sections extracted from the images in panel (e) and (f).

in agreement with earlier studies of CdSe nanostructures.[26,27] Figure 2b shows a photoluminescence (PL) spectrum of the nanobelt excited at 630 nm and recorded by steering the backscattered light into a spectrometer. The PL spectrum of the nanobelt shows an emission band peaking at 705 nm, indicating a slight modification of electronic structure from that of bulk CdSe due to the confined dimensions and high surface-to-volume ratio of the nanobelt.[28] Figure 2b also shows the wavelength dependence of the TA signal at the center of the nanobelt. Absorption bleaching (positive TA) dominates between 660 and 720 nm, and induced absorption (negative TA) is found at longer wavelengths with a maximum in magnitude at 730 nm. Induced absorption is also measured at wavelengths shorter than 660 nm. The TA spectrum thus highlights a competition between one- and two-photon absorption processes, respectively above and below the band edge (at ca. 730 nm), and an absorption by the photogenerated free carriers, as expected from a typical semiconductor.[16−22]

Band diagrams are presented in Figure 3 to illustrate further the excitation of carriers into the conduction band by the monochromatic picosecond pulses and the relevant absorption mechanisms influencing the TA. At longer wavelength (Figure 3a), when the photon energy is smaller than the band gap energy, charge carriers can be excited by two-photon absorption. At high pump fluence, a large density of transient free carriers is created by two-photon absorption to decay and populate the edge of the conduction band within a time scale typically less than a picosecond. A probe beam delayed from the pump is thus absorbed by intraband free carrier excitation, and the probed sample absorbance has increased from the irradiation with the pump, leading to a negative TA signal. At shorter wavelength (Figure 3b), when the photon energy is larger than the band gap energy, one-photon absorption is possible and induces accumulation of free carriers at the band edge. Carrier interband recombinations occur slowly within tens of picoseconds so that, when a probe pulse is delayed by only a few picoseconds from the pump, single-photon absorption is bleached. At low pump fluence, with little free carrier absorption, the probed absorbance is overall reduced. At very high pump fluence, large free carrier absorption leads to an overall absorbance increase. At even shorter wavelength (Figure 3c), single-photon absorption excites carriers far into the conduction band, and at high pump fluence a large free carrier density is created far into the band to decay within typically less than a picosecond at the band edge. With no carrier population preventing single-photon absorption, a probe beam delayed from the pump by several picoseconds is thus absorbed by single-photon and free carrier absorption. The probed sample absorbance is thus increased from the irradiation with the pump, leading to a negative TA signal.

In the experiments, at wavelengths between 660 and 720 nm, the one-photon absorption is thus bleached by a buildup of the excited carrier population, and the absorption bleaching dominates. However, the induced absorption dominates at shorter wavelengths because of the faster (femtosecond) intraband cooling of the population, which makes the bleaching less efficient. As shown in Figure 2e, at large pump powers (above 90 nW), induced absorption by free carriers also overwhelms the absorption bleaching near the band edge. Line profiles of the TA signal measured across the nanobelts at different wavelengths (Figure 2c) and pump intensities (Figure 2f) further reveal the competition between absorption bleaching and induced absorption. The variation of TA signal as a function of beam position across the nanobelts (Figure 2c and f) suggests that both linear and nonlinear properties of the TA signal can be exploited for manipulating the TA images, with for example the width of the TA profile at 50 nW being ca. 3 times larger than that of the dip in the TA measured at 110 nW (Figure 2f).

Figure 4a–c show backscattered images and corresponding line profiles of a single CdSe nanobelt at 679 nm (NB1, same nanobelt as shown in Figure 2a). These images were taken using circular polarized Gaussian and doughnut beams but without the detector polarizer (LP in Figure 1b). Insets show images of a single gold nanoparticle drop-cast on a glass slide. These images were recorded using the same imaging conditions as used for imaging CdSe. The full width at half-maximum (fwhm) of the nanoparticle in the Gaussian backscattered image is 400 ± 10 nm, which is marginally larger than the microscope diffraction-limited resolution of 380 nm expected from $\lambda/2NA$, and also accounts for the nanoparticle dimensions. The central node fwhm of the same nanoparticle

DOI: 10.1021/acsphotonics.5b00716
ACS Photonics 2016, 3, 478−485

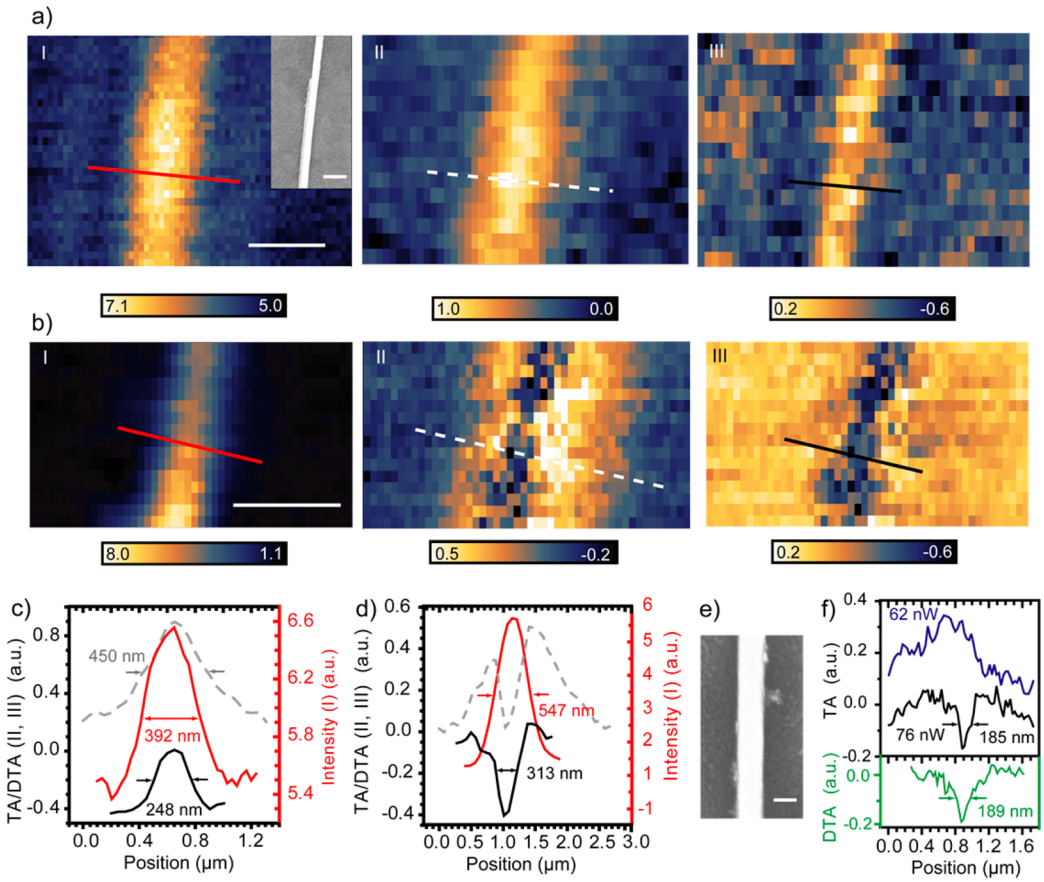

Figure 5. Backscattered, TA, and DTA image dependence on nanobelt physical dimensions and nonlinearity threshold. (a) I: Backscattered image of the nanobelt NB2 (scale bar 500 nm). The inset shows a scanning electron micrograph (SEM) of NB2 with a scale bar of 100 nm. II, III: TA and DTA images of the NB2 (Gaussian pump = 57 nW; doughnut pump = 61 nW; probe = 23 nW). (b) I, II, III: Backscattered, TA, and DTA images of the nanobelt NB3 at a pump power above the induced absorption threshold (130 nW; 65 nW; 10 nW). Scale bar is 1 μm. (c) Line profiles extracted from (a). (d) Line profiles extracted from (b). (e) SEM micrograph of NB4 with a scale bar of 50 nm. (f) TA line profiles across NB4 at two Gaussian pump intensities indicated in the plot and DTA line profile after subtraction of TA at these two intensities. The line profiles are offset for clarity.

imaged with the doughnut beam is 305 ± 10 nm. This value highlights that a differential scheme based on the two pump beam profiles will increase the optical performances of the microscopy.[11,12] The nodal geometry of the vortex-modified beam also justifies the depression at the center of the nanobelt in Figure 3b. Finite-element simulations of Gaussian backscattered images were performed to estimate the dimensions of the nanobelts from the optical images (see Supporting Information S3 and S4). NB1 in Figure 4a is measured as a protrusion with a fwhm of 483 ± 10 nm in the Gaussian backscattered image, and its physical width is estimated to be 220 ± 50 nm.

Both TA and DTA microscopies were performed at a fixed probe delay of ca. 4 ps as a compromise for the maximum transient signal and the suppression of interference between the probe and pump pulses. As discussed previously, the DTA microscopy scheme relies on alternating the pump intensity profile and/or power. TA images of NB1 were recorded in the absorption bleaching regime (<90 nW) at 679 nm using only a Gaussian pump (Figure 4e), only a doughnut pump (Figure 4f), and both these pumps in alternation in order to achieve DTA microscopy (Figure 4g). The fwhm measured in the Gaussian-pumped TA image is 847 ± 10 nm, while it is only 269 ± 10 nm for the DTA image (Figure 4h). DTA thus shows a clear improvement over TA and backscattered images. The DTA fwhm is a little above the value of ca. 240 nm computed for a nanobelt of width 220 nm (see Supporting Information S1). The discrepancy is expected from the Gaussian and doughnut intensity profiles departing from ideality in the experiment as well as from the simplicity of the model. The large fwhm measured for the Gaussian TA image in comparison to that measured on the Gaussian backscattered image comes from the polarization scheme used to limit the pump beam intake by the detector when performing the wavelength-degenerate TA microscopy (see Figure 4d and Methods). The combined effect of WP3 and LP prevents indeed a uniform detection of all polarization components of the probe field reflected/backscattered by the glass substrate and the nanobelt (see Supporting Information S5). The effect is strongly dependent on the WP3 and LP alignment so that the width in TA cannot be simply correlated with NB dimensions. Importantly, DTA images are only marginally affected since by adjusting the relative power between the two pumps, the differential signal is made to cancel away from the nanobelt and, thus, primarily reveals the difference in absorbance induced by the two pumps' illumination pattern on the sample.

TA and DTA microscopies were also performed on other individual CdSe nanobelts. Data on three of these (NB2, NB3, NB4) are shown in Figure 5. Other examples (NB5 and NB6) are presented in the Supporting Information section S6. DTA

DOI: 10.1021/acsphotonics.5b00716
ACS Photonics 2016, 3, 478−485

microscopy is sensitive to the optical absorption of the semiconductor materials, and the DTA amplitude is therefore zero on the glass away from the nanobelts. The nanobelts are thus, in the linear bleaching regime, systematically imaged as protrusions with subwavelength resolution (Figure 5a). Scanning electron microscopy (SEM) measurements on NB2 reveal a physical width of 82 ± 3 nm (see inset of Figure 5a). The fwhm of the same nanobelt imaged by the Gaussian backscattered image is 392 ± 10 nm. For a nanobelt of 82 nm, the finite-element simulations suggest a backscattered image fwhm of 382 nm, revealing a good agreement with the experiment (see Supporting Information S4). For this thin nanobelt, the DTA measurement shows a fwhm of 248 ± 10 nm, which is just above the value of ca. 220 nm estimated from the model in Supporting Information S1 when the power is kept within the TA linear regime below p_0. The experimental DTA fwhm is thus equivalent to $\lambda/3.0NA$ for thin nanobelts.

Subwavelength DTA imaging based on the TA nonlinearity is expected when the Gaussian pump power is set above the nonlinearity threshold p_0 (see Supporting Information S1), and this is verified below with NB3 and NB4. Backscattered, TA, and DTA images of NB3 (the same nanobelt as in Figure 2d) are shown in Figure 5b. The fwhm in the backscattered image is 547 ± 10 nm, and the nanobelt physical width is estimated as 280 ± 50 nm from the finite-element simulations (Supporting Information S4). When setting the Gaussian pump below p_0 at a power of 44 nW, the DTA image recorded with alternating Gaussian and doughnut pumps exhibits a fwhm of 330 ± 10 nm (see Supporting Information S6), in line thus with the expectation that physically wider belts are also imaged larger by DTA. When the pump power is increased to 130 nW, above the nonlinearity threshold p_0, the TA image of NB3 exhibits a dip of half-width 313 ± 10 nm (Figure 5b). The dip relates to the transition from absorption bleaching to free-carrier-induced absorption. When DTA is performed, the image is that of a depression of the same half-width of 313 ± 10 nm and the differentiation essentially results in the suppression of the TA signal at large distance from the physical nanobelt, so that only the intense dip remains. Noteworthy, the dip is induced by the Gaussian pump beam and not from the doughnut pump. The small difference between the DTA width below and above p_0 is due to the physical width of the belt (280 ± 50 nm) being large with respect to the expected resolution. However, NB4 has a physical width of 56 ± 3 nm measured by SEM and exhibits a dip of ca. 185 nm ($\lambda/4.1NA$) in the TA line profile when the power is increased to 76 nW and shows no dip at 62 nW. The threshold p_0 for the thin NB4 is seen lower than for the thicker NB2 and NB3. This highlights the dependence of TA with respect to specimen properties and the subsequent need for collecting TA images at appropriate pump power in dispersed samples. Remarkably, the width of the dip for NB4 ($\lambda/4.1NA$) measured solely with a Gaussian pump above p_0 is less than the fwhm measured by DTA for the similarly thin NB2 in the linear regime below p_0 with a doughnut (see above, $\lambda/3.0NA$).

CONCLUSIONS

The imaging performances of DTA, below p_0 and by differentiation with a doughnut pump, are thus like those demonstrated by the RESOLFT-based TA microscopy exploiting absorption saturation on graphene nanoplatelets ($\lambda/3.0NA$), where the smallest fwhm is ca. 225 nm for an NA of 1.2 and an optical transition probed at 800 nm.[3] The similarity in the results despite the absence of saturation here stems from the ability to exploit a pump of the same wavelength as the probe, taking advantage thus of a relatively narrower node in the doughnut. With the saturation of a doughnut, the maximum resolution enhancement is essentially determined by the ratio between damage and saturation threshold. Noteworthy, if the TA saturates beyond p_0, increasing the doughnut pump power above this threshold should lead to further improvement in the resolution, in line with other RESOLFT-based approaches (see ref 10 and Supporting Information S1). On the other hand, the observation here for CdSe of a width of $\lambda/4.1NA$ using only Gaussian-shaped pumps of power a little above the transition threshold p_0 supports our proposition that super-resolution can be achieved also in the absence of TA saturation. Remarkably, the maximum resolution enhancement is here not limited by the ratio between damage and saturation thresholds, and, with TA nonlinearities widely observed in materials,[16−22] specimen photodamage is expected to be of a lesser concern. The sensitivity of the TA super-resolution method remains linked to that of any TA microscopy,[2,3,29] and in this work, the optical system allowed the analysis of nanobelts wider than 50 nm. Yet, the imaging of smaller objects by TA microscopy is possible and performances beyond those shown here are expected (see Supporting Information S7).

The ability to manipulate the TA images using nonlinearities such as optical saturation for graphene[3] or the opening of an additional absorption channel for CdSe is determined by the optical properties of the specimen, and thus the exploitation of these super-resolution schemes requires knowledge on the TA dependence with pump power at a given probe wavelength. In simple terms, to achieve optimum performances, probe wavelength and pump wavelength and power must be adjusted to the specimen absorption band that is targeted. It is expected however that the ability developed here to exploit a wavelength-degenerate scheme will facilitate the tuning of these parameters, as only two out of these three are relevant. Conversely, nonlinearities in TA do not have to be induced in degenerate conditions, and the exploitation of shorter pump wavelengths is also expected to improve the effective resolution.

In summary, a far-field, subdiffraction absorption microspectroscopy based on nonlinear transient absorption differential microscopy is demonstrated for CdSe nanobelts, with temporal and spectral structure common to a wide range of semiconductors. With the increasing importance of semiconductor nanomaterials in many areas of technologies such as nanomechanics,[30] photovoltaics,[31] optical lasers and amplifiers,[32,33] and integrated electronic and photonic circuits,[34,35] the realization of nondestructive, super-resolution far-field optical microscopy is an important step forward in implementing rapid, nondestructive spectral analysis of nanodevices. The DTA scheme will go beyond offering higher spatial resolution by revealing a label-free physical picture, more complete than can be recorded from scattering, and by also probing the temporal evolution of excited states at scale matching device nanofeatures. Due to its general applicability in super-resolution imaging of both semiconductors and insulators, DTA has the potential to become a necessary nanoscience tool for investigation, development, and control of current and emerging nanomaterials and devices.

DOI: 10.1021/acsphotonics.5b00716
ACS Photonics 2016, 3, 478−485

■ ASSOCIATED CONTENT

Supporting Information

The Supporting Information is available free of charge on the ACS Publications website at DOI: 10.1021/acsphotonics.5b00716.

Additional information (PDF)

■ AUTHOR INFORMATION

Corresponding Author

*E-mail: christophe.silien@ul.ie.

Notes

The authors declare no competing financial interest.

■ ACKNOWLEDGMENTS

The LANIR research leading to these results has received funding from the European Community's Seventh Framework Programme (FP7/2012-2015) under grant agreement no. 280804. This communication reflects the views only of the authors, and the Commission cannot be held responsible for any use that may be made of the information contained therein. This research was also supported by Science Foundation Ireland (13/TIDA/I2613). M.K. acknowledges funding from the Integrated Nanoscience Platform for Ireland (INSPIRE), initiated by the Higher Education Authority in Ireland within the PRTLI5 framework. I.P. acknowledges a postgraduate scholarship from the Irish Research Council (GOIPG/58/2013). A.P. is a Research Director of the Belgian Fund for Scientific Research (FNRS-FRS).

■ REFERENCES

(1) Hartland, G. V. Ultrafast studies of single semiconductor and metal nanostructures through transient absorption microscopy. *Chem. Sci.* **2010**, *1*, 303−309.

(2) Huang, L.; Hartland, G. V.; Chu, L.-Q.; Luxmi; Feenstra, R. M.; Lian, C. X.; Tahy, K.; Xing, H. L. Ultrafast Transient Absorption Microscopy Studies of Carrier Dynamics in Epitaxial Graphene. *Nano Lett.* **2010**, *10*, 1308−1313.

(3) Wang, P.; Slipchenko, M. N.; Mitchell, J.; Yang, C.; Potma, E. O.; Xu, X. F.; Cheng, J.-X. Far-field imaging of non-fluorescent species with subdiffraction resolution. *Nat. Photonics* **2013**, *7*, 449.

(4) Min, W.; Lu, S. J.; Chong, S. S.; Roy, R.; Holtom, G. R.; Xie, X. S. Imaging chromophores with undetectable fluorescence by stimulated emission microscopy. *Nature* **2009**, *461*, 1105.

(5) Hell, S. W.; Wichmann, J. Breaking the diffraction resolution limit by stimulated emission: stimulated-emission-depletion fluorescence microscopy. *Opt. Lett.* **1994**, *19*, 780−782.

(6) Klar, T. A.; Jakobs, S.; Dyba, M.; Egner, A.; Hell, S. W. Fluorescence microscopy with diffraction resolution barrier broken by stimulated emission. *Proc. Natl. Acad. Sci. U. S. A.* **2000**, *97*, 8206−8210.

(7) Maurer, P. C.; Maze, J. R.; Stanwix, P. L.; Juang, L.; Gorshkov, A. V.; Zibrov, A. A.; Harke, B.; Hodges, J. S.; Zibrov, A. S.; Yacoby, A.; Twitchen, D.; Hell, S. W.; Walsworth, R. L.; Lukin, M. D. Far-field optical imaging and manipulation of individual spins with nanoscale resolution. *Nat. Phys.* **2010**, *6*, 912.

(8) Rittweger, E.; Han, K. Y.; Irvine, S. E.; Eggeling, C.; Hell, S. W. STED microscopy reveals crystal colour centres with nanometric resolution. *Nat. Photonics* **2009**, *3*, 144−147.

(9) Chu, S.-W.; Su, T.-Y.; Oketani, R.; Huang, Y.-T.; Wu, H.-Y.; Yonemaru, Y.; Yamanaka, M.; Lee, H.; Zhuo, G.-Y.; Lee, M.-Y.; Kawata, S.; Fujita, K. Measurement of a Saturated Emission of Optical Radiation from Gold Nanoparticles: Application to an Ultrahigh Resolution Microscope. *Phys. Rev. Lett.* **2014**, *112*, 017402.

(10) Heintzmann, R. Beyond the realm of fluorescence. *Nat. Photonics* **2013**, *7*, 425−428.

(11) Silien, C.; Liu, N.; Hendaoui, N.; Tofail, S. A. M.; Peremans, A. A framework for far-field infrared absorption microscopy beyond the diffraction limit. *Opt. Express* **2012**, *20*, 29694−29704.

(12) Pita, I.; Hendaoui, N.; Liu, N.; Kumbham, M.; Tofail, S. A. M.; Peremans, A.; Silien, C. High resolution imaging with differential infrared absorption micro-spectroscopy. *Opt. Express* **2013**, *21*, 25632.

(13) Haeberlé, O.; Simon, B. Saturated structured confocal microscopy with theoretically unlimited resolution. *Opt. Commun.* **2009**, *282*, 3657−3664.

(14) Kuang, C. F.; Li, S.; Liu, W.; Hao, X.; Gu, Z. T.; Wang, Y. F.; Ge, J. H.; Li, H. F.; Liu, X. Breaking the Diffraction Barrier Using Fluorescence Emission Difference Microscopy. *Sci. Rep.* **2013**, *3*, 1441.

(15) Sheppard, C. J. R.; Wilson, T. Image formation in confocal scanning microscope. *Optik* **1980**, *55*, 331.

(16) Motamedi, A. R.; Nejadmalayeri, A. H.; Khilo, A.; Kartner, F. X.; Ippen, E. P. Ultrafast nonlinear optical studies of silicon nanowaveguides. *Opt. Express* **2012**, *20*, 4085.

(17) Langlois, P.; Joschko, M.; Thoen, E. R.; Koontz, E. M.; Kartner, F. X.; Ippen, E. P.; Kolodziejski, L. A. High fluence ultrafast dynamics of semiconductor saturable absorber mirrors. *Appl. Phys. Lett.* **1999**, *75*, 3841.

(18) Robel, I.; Bunker, B. A.; Kamat, P. V.; Kuno, M. Exciton Recombination Dynamics in CdSe Nanowires: Bimolecular to Three-Carrier Auger Kinetics. *Nano Lett.* **2006**, *6*, 1344−1349.

(19) Kambhampati, P. Hot Exciton Relaxation Dynamics in Semiconductor Quantum Dots: Radiationless Transitions on the Nanoscale. *J. Phys. Chem. C* **2011**, *115*, 22089−22109.

(20) Gundlach, L.; Piotrowiak, P. Ultrafast Spatially Resolved Carrier Dynamics in Single CdSSe Nanobelts. *J. Phys. Chem. C* **2009**, *113*, 12162−12166.

(21) Zhang, J. Z. Interfacial Charge Carrier Dynamics of Colloidal Semiconductor Nanoparticles. *J. Phys. Chem. B* **2000**, *104*, 7239−7253.

(22) Yumashev, K. V.; Prokoshin, P. V.; Malyarevich, A. M.; Mikhailov, V. P. Transient bleaching/induced absorption in reduced $SrTiO_3$ under picosecond excitation. *J. Opt. Soc. Am. B* **1997**, *14*, 415.

(23) Liu, C.; Wu, P. C.; Sun, T.; Dai, L.; Ye, Y.; Ma, R. M.; Qin, G. G. Synthesis of High Quality n-type CdSe Nanobelts and Their Applications in Nanodevices. *J. Phys. Chem. C* **2009**, *113*, 14478−14481.

(24) Singh, A.; Gunning, R. D.; Ahmed, S.; Barrett, C. A.; English, N. J.; Garate, J.-A.; Ryan, K. M. Controlled semiconductor nanorod assembly from solution: influence of concentration, charge and solvent nature. *J. Mater. Chem.* **2012**, *22*, 1562−1569.

(25) Gur, I.; Fromer, N. A.; Geier, M. L.; Alivisatos, A. P. Air-Stable All-Inorganic Nanocrystal Solar Cells Processed from Solution. *Science* **2005**, *310*, 462−465.

(26) Junnarkar, M. R.; Alfano, R. R. Photogenerated high-density electron-hole plasma energy relaxation and experimental evidence for rapid expansion of the electron-hole plasma in CdSe. *Phys. Rev. B: Condens. Matter Mater. Phys.* **1986**, *34*, 7045−7062.

(27) Burda, C.; Link, S.; Green, T. C.; El-Sayed, M. A. New Transient Absorption Observed in the Spectrum of Colloidal CdSe Nanoparticles Pumped with High-Power Femtosecond Pulses. *J. Phys. Chem. B* **1999**, *103*, 10775−10780.

(28) Tamargo, M. C. *Optoelectronic Properties of Semiconductors and Superlattices - II-VI Semiconductor Materials and their Applications*, Vol. *12*; Taylor and Francis, 2002.

(29) Lo, S. S.; Devadas, M. S.; Mahor, T. A.; Hartland, G. V. Optical detection of single nano-objects by transient absorption microscopy. *Analyst* **2013**, *138*, 25.

(30) Liu, N.; Giesen, F.; Belov, M.; Losby, J.; Moroz, J.; Fraser, A. E.; McKinnon, G.; Clement, T. J.; Sauer, V.; Hiebert, W. K.; Freeman, M. R. Time Domain Control of Ultrahigh Frequency Nanomechanical Systems. *Nat. Nanotechnol.* **2008**, *3*, 715.

(31) Robel, I.; Subramanian, V.; Kuno, M.; Kamat, P. V. Quantum Dot Solar Cells. Harvesting Light Energy with CdSe Nanocrystals Molecularly Linked to Mesoscopic TiO_2 Films. *J. Am. Chem. Soc.* **2006**, *128*, 2385−2393.

DOI: 10.1021/acsphotonics.5b00716
ACS Photonics 2016, 3, 478−485

(32) Berini, P.; De Leon, I. Surface plasmon-polariton amplifiers and lasers. *Nat. Photonics* **2012**, *6*, 16−24.
(33) Liu, N.; Wei, H.; Li, J.; Wang, Z. X.; Tian, X. R.; Pan, A. L.; Xu, H. X. Plasmonic Amplification with Ultra-High Optical Gain at Room Temperature. *Sci. Rep.* **2013**, *3*, 1967.
(34) Whang, D.; Jin, S.; Wu, Y.; Lieber, C. M. Large-Scale Hierarchical Organization of Nanowire Arrays for Integrated Nanosystems. *Nano Lett.* **2003**, *3*, 1255−1259.
(35) Heck, M. J. R.; Chen, H. W.; Fang, A. W.; Koch, B. R.; Liang, D.; Park, H.; Sysak, M. N.; Bowers, J. E. Hybrid Silicon Photonics for Optical Interconnects. *IEEE J. Sel. Top. Quantum Electron.* **2011**, *17*, 333−346.

DOI: 10.1021/acsphotonics.5b00716
ACS Photonics 2016, 3, 478−485